Title:

Evaluation of Arcjet Type Atomic Oxygen Generator

Authors:

Makoto Matsui [a]*, Hiroki Takayanagi [b], Yasuhisa Oda [a], Kimiya Komurasaki [a] and Yoshihiro Arakawa [b]

Affiliations:

[a] Department of Advanced Energy, The University of Tokyo

[b] Department of Aeronautics and Astronautics, The University of Tokyo

Hongo 7-3-1, Bunkyo, Tokyo 133-8656, Japan

* *Coresponding Author:*

Makoto Matsui

Department of Advanced Energy, The University of Tokyo

Hongo 7-3-1, Bunkyo, Tokyo 133-8656, Japan

Fax: 03-5841-6586

Email: matsui@al.t.u-tokyo.ac.jp

Abstract:

The performance of arcjet type arc-heater as an atomic oxygen generator developed at the University of Tokyo was evaluated by laser absorption spectroscopy and CFD simulation. As a result, degree of dissociation of oxygen is found unexpectedly small at the level of 0.01% due to the slow mixing processes of oxygen with the inert gas heated by arc discharge in the constrictor.

Keywords:

Arcjet type arc-heater, Atomic oxygen, Laser absorption spectroscopy

1. Introduction

In developing Thermal Protection Systems for reentry vehicles such as the space shuttle, arcjet type arc-heaters are often used to experimentally simulate reentry conditions because they can operate for several hours continuously with minimum maintenance effort. [1,2] Recently, atomic oxygen in the plumes is found to play important roles in TPS tests through the heat-flux enhancement by catalytic effect and the active-passive oxidation of TPS surfaces [3,4]. Therefore, arcjet type arc-heaters come to be used as an atomic oxygen generator.

However, their exact plume conditions are mostly unknown because they are usually in strong thermo-chemical non-equilibrium. Although non-intrusive spectroscopic methods such as emission spectroscopy and Laser Induced Florescence spectroscopy have been actively applied to the characterization of such high enthalpy plumes, [5,6] it is still difficult to measure the chemical compositions by these spectroscopic methods.

In this study, laser absorption spectroscopy and CFD simulation are applied to estimate the degree of dissociation of oxygen in the arcjet type arc-heater plumes and its performance as an atomic oxygen generator is evaluated.

2. Experimental Method and Apparatus

2.1 Laser absorption spectroscopy

Laser absorption spectroscopy is applicable to optically thick plasma and does not require absolute calibration using a calibrated light source or a density reference cell. In addition, measurement system using a diode laser can be portable [7,8].

The relationship between laser intensity I_ν and absorption coefficient $k_\nu(x)$ is expressed by the Beer-Lambert law as,

$$\frac{\mathrm{d}I_\nu}{\mathrm{d}x} = -k_\nu(x) I_\nu . \tag{1}$$

Here, ν is the laser frequency and x is the coordinate in the laser pass direction. Because distributions of absorption properties in plumes would be axisymmetric, local absorption coefficient $k_\nu(r)$ is obtained by the Abel inversion.

Assuming Boltzmann relation between absorbing and excited states, integrated absorption coefficient $K(r)$ is expressed as a function of the number density at the absorbing state $n_i(r)$ as,

$$K(r) = \int_{-\infty}^{\infty} k_\nu(r)\mathrm{d}\nu = \frac{\lambda^2}{8\pi}\frac{g_j}{g_i} A_{ji} n_i(r)\left[1-\exp\left(-\frac{\Delta E_{ij}}{kT_{\mathrm{ex}}}\right)\right]. \tag{2}$$

Here, subscripts 'i' and 'j' denote the absorbing and excited states, respectively. λ, g, A, ΔE, k and T_{ex} are the absorption wavelength, statistical weight, Einstein coefficient, energy gap between the states, Boltzmann constant and electronic excitation

temperature, respectively. Transition data of target absorption lines in this study are listed in Table1. $\Delta E_{ij}/kT_{ex}$ was so large in the plumes that stimulated emission can be neglected and Eq.(2) is approximated as,

$$K(r) = \frac{\lambda^2}{8\pi} \frac{g_j}{g_i} A_{ji} n_i(r). \quad (3)$$

2.2 Experimental apparatus

2.2.1 Arc-heater

The schematic of arcjet type arc-heater developed at the University of Tokyo is shown in Fig.1. As seen in this figure, inert gas (argon is used in this experiment) is supplied from the base of cathode rod and oxygen is added at the constrictor part to prevent the cathode from oxidization. The flow Mach number of the plume was designed at 2. The thermal efficiency was estimated about 60% by measuring the increase in cooling water temperature. The input power, gas flow rates, specific enthalpy and ambient pressure were 1.1kW, argon 6slm, oxygen 1slm, 3.6MJ/kg and 53Pa, respectively.

2.2.1 Measurement system

The measurement system is shown in Fig. 2. A tunable diode-laser with an external

cavity was used as a probe and an ethalon, whose free spectral range is 1 GHz, was used as a wavemeter. Probe beam was lead to a window of vacuum chamber through a multimode optical fiber. The fiber output was mounted on a one-dimensional traverse stage to scan the plume in the radial direction. At the other side of the chamber, the probe beam was focused on a photo-detector using a parabola mirror. This made it possible to detect the probe beam without synchronizing the detector position with the laser scanning. A photograph of the plume with measured planes is shown in Fig.3.

3. Experimental Results and Discussion

The number density distribution of O at the absorbing state is shown in Fig.4. Here, (r, z) is the cylindrical coordinate and its origin is taken at the center of the nozzle exit. At z=0mm, the peak of number density was located off axis at r=11mm. Then, in the downstream of the plume, the peak was shifted to the axis and the density was increased. The maximum number density was $3.5\times10^{16}m^{-3}$ at z=60mm.

Figure 5 shows the number density distribution of Ar at the absorbing state. It had a peak of $3.0\times10^{17}m^{-3}$ on the axis at z=0mm and then the peak was decreased monotonically in the downstream of the plume.

Consequently, it is thought that oxygen was localized off axis near the nozzle exit

and diffused toward the axis in the downstream region while being dissociated by the collisions with argon. Oxygen would not be enough mixed with hot argon in the constrictor region. The hypothetical argon-oxygen mixing processes in the plume are schematically shown in Fig. 6.

4. Analytical Method and Models

The O number density at the ground state is difficult to be estimated from that at the absorbing state because the energy level of the absorbing state is far above that of the ground state. Therefore, total O number density and its distribution were simulated by CFD analysis in the constrictor, nozzle and the plume.

4.1 Numerical models

Arc discharge process has not been solved for simplicity because this simulation focuses on the diffusion and mixing processes of the oxygen injected into the inert gas flow at the constrictor part. The temperature distribution of argon inlet flow was given as a boundary condition assuming thermo-chemical equilibrium because the flow speed is subsonic and pressure is high around the cathode tip.

Seven species and seven chemical reactions are taken into account as listed in Table 2. Arrehenius type forward reaction rates were used and the principle of the

detailed balance was used to have backward reaction rates. [9] One temperature model is employed. Transport coefficients such as viscosity, thermal conductivity and diffusion coefficient were calculated by the formulas in reference 1o. The algebraic turbulence model by the Plandtl's mixing length theory was used. [11] The Reynolds number in the free-jet region was 1800.

4.2 Governing equations and computational method

The governing equations are two-dimensional axisymmetric Navier-Stokes equations extended to chemical non-equilibrium gases. The convection terms were calculated using the SHUS (Simple High-resolution Upwind Scheme, [12]) in which the spatial accuracy is extended to third order using the MUSCL approach. Implicit time integration has been done using the LU-SGS (Lower-Upper Symmetric Gauss Seidel Scheme. [13])

4.3 Computational grids and conditions

The schematic of computational grid is shown in Fig.7. The calculation region is composed of the constrictor-nozzle section and the free jet section. At the interface of these sections, several computational grids were superposed to preserve the spatial

accuracy. It was not necessary to concentrate the grid points near the wall surface, because entire region in the constrictor and nozzle is covered by boundary layers.

The grid spacing in the radial direction Δr should be so small that the numerical dissipation effect is smaller than actual diffusion. To have a grid convergence, Δr was set at 1.3mm and total number of grid points was about 10,000.

The same operational conditions as those in the experiment were computed. Subsonic inflow conditions are employed for the inlets of constrictor and of oxygen injection slit. To simulate the cathode jet phenomenon, Gaussian temperature distribution was assumed at the inlet as shown in Fig.8. The degree of ionization of argon at the inlet was computed assuming the Saha equilibrium. As for the wall of the constrictor and nozzle, adiabatic non-slip wall conditions were adopted.

5. Analytical Results and Discussion

The radial distributions of O_2 and O mole-fraction at the constrictor exit are shown in Fig.9 along with the temperature distribution. Oxygen mixing is very slow and it is localized at outer side of the plume in the constrictor. Although the degree of dissociation is very high near the axis due to the high temperature cathode jet, O mole-fraction is very small.

O number density distributions are shown in Fig.10. As seen in this figure, the peak is located off axis at z=0~30mm and on axis in the downstream of the plume, similarly to that in Fig.4.

Consequently, this slow mixing process would be the reason why the measured distribution O at the absorbing state has a peak off axis at the nozzle exit. Although the oxygen is mixed gradually in the plume, the reaction rate is quite small there because of the decrease in temperature: In the plume, computed temperature is the level of 2,000 K on the axis. The volume-averaged degree of dissociation is estimated at 0.01%.

As mentioned above, oxygen dissociation is hardly expected in the plume of the arcjet type arc-heater. Therefore, it is necessary to promote the mixing in the constrictor region to achieve high O number density in the plume.

6. Conclusion

O number density in the arcjet type arc-heater plume was obtained by laser absorption spectroscopy and CFD simulation. As a result, oxygen injected at the constrictor was found not enough mixed with argon, resulting in the quite small degree of dissociation of oxygen in the plume. Therefore, for the enhancement of the oxygen dissociation, the oxygen injection-port should be improved to promote the mixing

between oxygen and argon.

References

[1] Nishida M, et.al.; *Trans. Jpn. Soc. Aeronaut. Space Sci.*, 1998, 31, p123-133.

[2] Auweter-Kurtz M, et.al.;, *J. Propulsion Power*, 1996, 12, p1053-1061.

[3] Kurotaki T.; *AIAA Paper* 2000-2366, 2000.

[4] Laux T, et.al.; *AIAA Paper* 2001-3020, 2001.

[5] Lago V, et.al.; *J Thermophys. Heat Transfer*, 2001, 15, p168-175.

[6] Storm P, et.al.; *AIAA Paper* 95-2381, 1995.

[7] Arroyo M, et.al.; *Appl. Opt.*, 1994, 33, p3296-3370.

[8] Matsui M, et.al.; *Appl. Plasma Sci.*, 2001, 9, p17-22.

[9] Matsuzaki R.; *Trans. Jpn. Soc. Aeronaut. Space Sci.*, 1988, 30, p243-258.

[10] Guputa R. N, et.al.; *NASA RP* 1232, 1990.

[11] Wilcox, D. C.; *DCW Industries*, California, 1993

[12] Shima E, et.al.; *NAL SP* 34, 1997, p7-12.

[13] Jameson A, et.al.; *AIAA J.*, 1988, 25, p929-935.

Figure Captions;

Fig.1 The University of Tokyo arcjet type arc-heater (upper) and the zoom up of constrictor part (below.)

Fig.2 Measurement system.

Fig.3 Photograph of arc-heater plume and measurement planes.

Fig.4 Number density distribution of O at the absorbing state in arc-heater plume.

Fig.5 Number density distribution of Ar at the absorbing state in arc-heater plume.

Fig.6 Hypothetical argon-oxygen Mixing process.

Fig.7 Computational grid.

Fig.8 Gas inlet conditions.

Fig.9 Contours of the computed gas properties in the constrictor.

Fig.10 Computed O density distribution in arc-heater plume.

Table captions:

Table 1 Transition data

Table 2 Chemical reaction models.

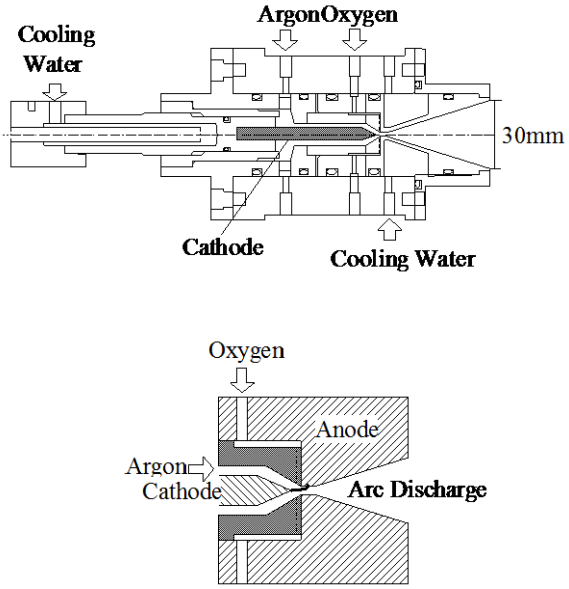

Fig.1 The University of Tokyo arcjet type arc-heater (upper) and the zoom up of constrictor part (below.)

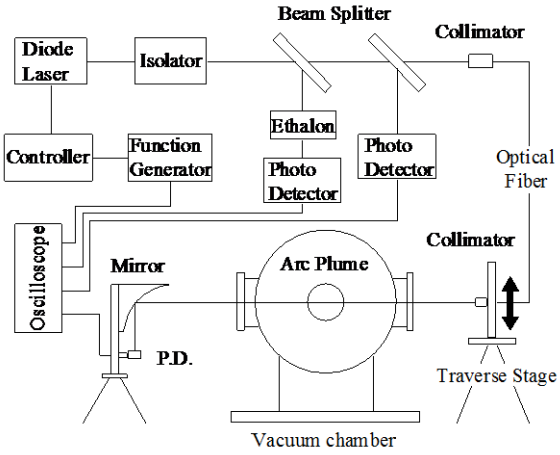

Fig.2 Measurement system.

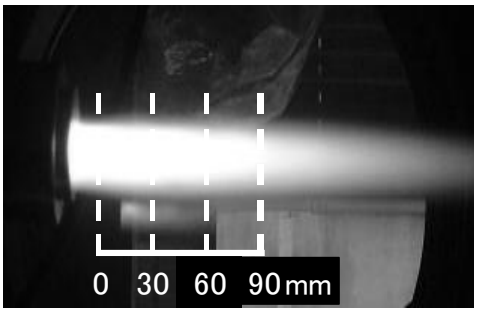

Fig.3 Photograph of arc-heater plume and measurement planes.

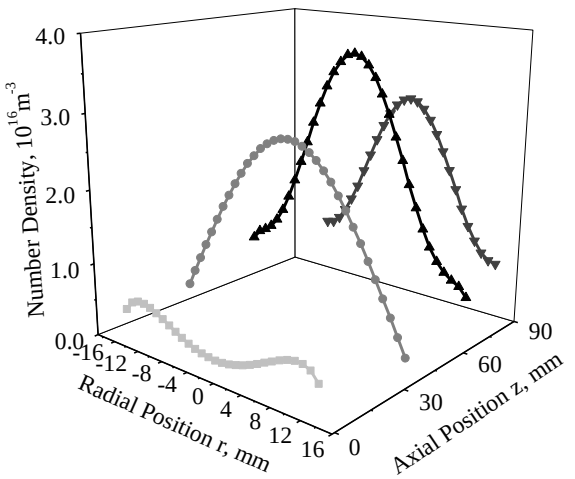

Fig.4 Number density distribution of O at the absorbing state in arc-heater plume.

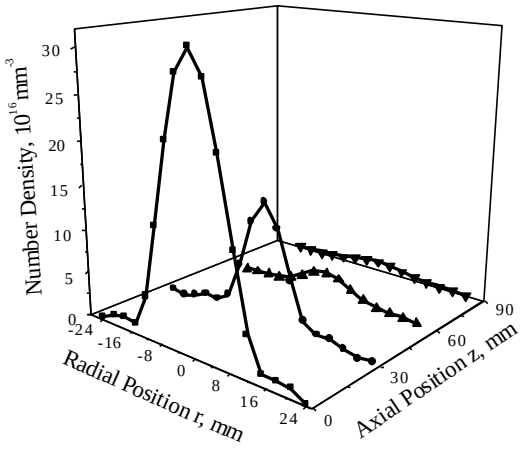

Fig.5 Number density distribution of Ar at the absorbing state in arc-heater plume.

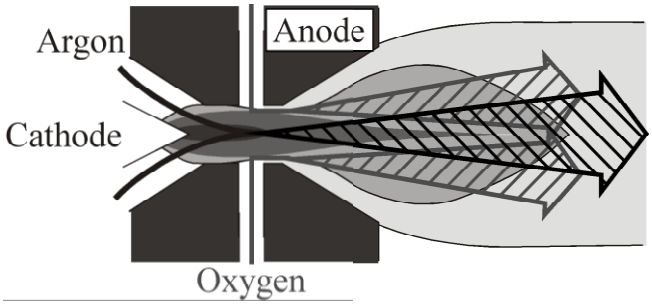

Fig.6 Hypothetical argon-oxygen Mixing process.

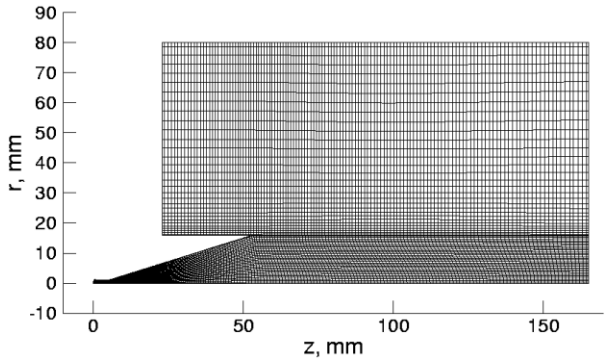

Fig.7 Computational grid.

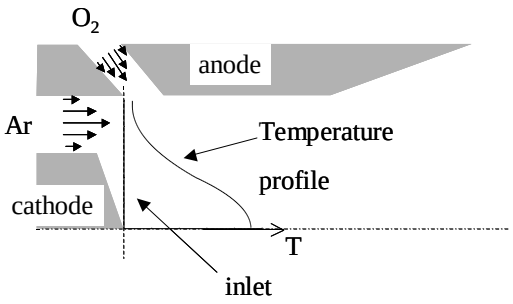

Fig.8 Gas inlet conditions.

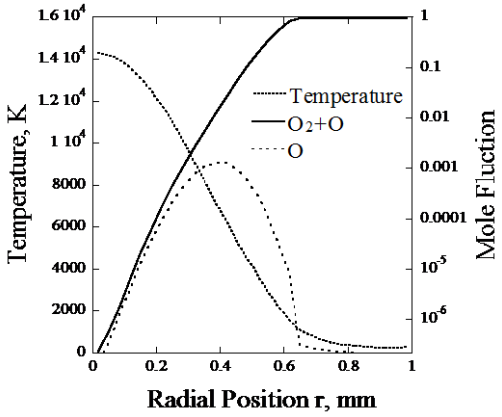

Fig.9 Contours of the computed gas properties in the constrictor.

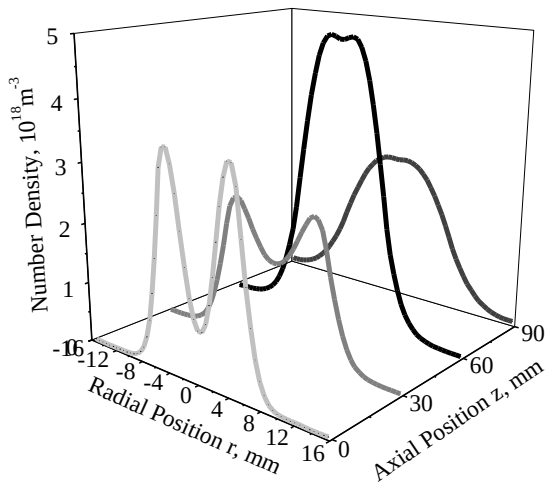

Fig.10 Computed O density distribution in arc-heater plume.

Table 1 Transition data

	i	j	λ(nm)	E_i (eV)	E_j (eV)	g_i	g_j	$A_{ji}(10^8 s^{-1})$
OI	$3s^5S$	$3p^5P$	777.19	9.14	10.7	5	7	0.369
ArI	$4s^2[1/2]$	$4p^2[3/2]$	840.82	11.8	13.3	3	5	0.223

Table 2 Chemical reaction models.

Reaction process
$Ar + e \Leftrightarrow Ar^{+} + e +$
$O_2 + Ar \Leftrightarrow O + O$
$O_2 + O \Leftrightarrow O + O +$
$O_2 + O_2 \Leftrightarrow O + O +$
$O + e \Leftrightarrow O^{+} + e + e$
$O + O \Leftrightarrow O_2^{+} + e$
$O + O_2^{+} \Leftrightarrow O_2 + O^{+}$